

Evaluation of the 3D compositional heterogeneity effect on line-edge-roughness [§]

Shuhui Kang^a, Wen-li Wu *^a, Vivek M. Prabhu^a, Bryan D. Vogt^a, Eric K. Lin^a,
Karen Turnquest^b,

^aPolymers Division, National Institute of Standards and Technology,
Gaithersburg, MD, 20899

^bSEMATECH, 2706 Montopolis Dr, Austin, Texas 78741

Abstract

The controlling factors in the formation of the compositional heterogeneity at the deprotection front were investigated using 3D computer simulation. The results illustrate that the chemical composition fluctuation (CCF) formed by the photoresist deprotection reaction is an important factor contributing to the line-edge-roughness (LER) in addition to the deprotection gradient (DG) of the reaction front. The magnitude of the chemical composition fluctuation and the deprotection gradient are found to depend on the ratio of the deprotection reaction rate constant to diffusion coefficient (k_p/D) and the number of hopping step (n). With this new finding, the influence on LER from various process/material parameters such as dose/contrast, diffusivity, and reactivity can all be understood through their effects on k_p/D and n .

1. Introduction

As the feature line size of integrated circuits approaches 45 nm, the magnitude of LER must be below ≈ 2 nm to ≈ 3 nm as specified by the international technology roadmap for semiconductor (ITRS). This dimension has approached the size of individual polymer chains of chemically amplified (CA) photoresists. Due to the recent developments in immersion lithography and overwhelming advantages on sensitivity and throughput over other alternatives chemically amplified photoresists remain a crucial enabler for the semiconductor industry.

This work is aimed at unraveling the effects of various processing and material parameters on LER. It is well known that LER is strongly process and materials dependent ¹. Besides the composition of the photoresist polymer, photoacid generator (PAG) and base quencher almost all the intermediate processing steps play a role on the final LER such as exposure²⁻⁴, post-exposure bake (PEB)^{5,6} and development⁷⁻⁹. Due to the large number of variables, we chose to perform 3D computer simulations to identify and explore general correlations between LER and these parameters. The development physics is not included in the present work, hence, LER in the present context is analogy to chemical compositional roughness at the solubility switch.

Many previous work on photoresists modeling and LER have been reported, ¹⁰⁻¹⁵ however, a general picture of how the LER is related to processing and materials parameters is still missing. This work is built upon a recent finding that a simple empirical relation exists between LER and the gradient of deprotection reaction profile^{16,3}. It was observed that the LER from various processing conditions forms a master curve when plotted against the gradient. Even though significant scatter occurs along the master curve depending on base quencher concentration and resist polymer type, this finding significantly reduced the parameters to be considered for LER minimization. It also provokes an important question; what governs this monotonic relationship between LER and the deprotection gradient?

[§] Official contribution of the National Institute of Standards and Technology; not subject to copyright in the United States

* Corresponding author. E-mail: wenli@nist.gov

2. Simulation methodology

In this study, we apply a model in calculating the LER by combining macroscopic photoacid diffusion law and reaction kinetics with the microscopic reaction-diffusion picture based on a random-walk and molecular collision mechanism.

2.1 Chemical latent image calculation

A combination of a diffusion equation and first order reaction kinetics are the starting point for our modeling effort.

$$\text{Photoacid generation:} \quad H = PAG_0(1 - e^{-CE}) \quad (1)$$

$$\text{Deprotection reaction:} \quad \frac{d\phi}{dt} = k_p H(1 - \phi) \quad (2)$$

$$\text{Photoacid diffusion and trapping:} \quad \frac{\partial H}{\partial t} = D\nabla^2 H - k_T H\phi \quad (3)$$

Here the C and E are Dill parameter and the exposure dose, respectively. The H and ϕ are the photoacid concentration and the deprotection level which both have time and position dependence. The D , k_p and k_T are the diffusion coefficient of photoacid, the deprotection reaction constant and acid trapping constant, respectively. The trapping factor is introduced to reflect the acid loss due to the hydrogen bonding interaction between photoacid and reaction product¹⁷. The introduction of k_T also accounts for the non-Fickian diffusion behavior observed in many deprotection reactions. Base quencher is not considered here, but can be included through additional acid loss terms. In this work, the experimental parameters used in Pawloski et al.³ are used as the standard or starting condition as listed in Table 1.

In our macroscopic reaction-diffusion calculation both the PAG distribution and the dose are assumed to be varied only in one direction – the x-axis, the above equations are considered to be one dimensional. A boundary condition with zero flux across the boundary is used to solve the partial differential equations. A Matlab code is employed to perform the 1D calculation and the 3D simulation to be discussed hereafter.

The above equations provide a continuous and smooth solution for the deprotection level. At a microscopic or a molecular level we consider that the deprotection reaction is a result of collision of a moving photoacid with fixed acid-labile protection moieties. The deprotection level ϕ is a statistical average produced by many individual photoacids. Therefore the chemical image roughness is attributed to fluctuations in photoacid concentration. If we assume each photoacid randomly hops within the uniform polymer matrix at a constant frequency (Figure 1), the probability of the photoacid appearing in a given position or the distribution of the photoacid concentration follows the Fickian law, which is given by

$$\rho(r, t) = (4\pi Dt)^{-3/2} e^{-r^2/4Dt} \quad (4)$$

Where “ r ” is the distance between the origin of a PAG and a given point. The “ t ” is the total hopping time and “ D ” is the apparent diffusion coefficient. The point blur function (PBF) which is produced by the diffusion-reaction of a single PAG can then be obtained by inserting equation (4) into equation (2) and solving the differential equation.

$$PBF = 1 - \exp[-(k_p / 4\pi D) \text{erfc}(r / \sqrt{4Dt}) / r] \quad (5)$$

Here a boundary condition that the deprotection level is equal to zero at $r = \infty$ has been used. Surprisingly, this is not a Gaussian or Lorentzian function about the “ r ” as expected, but it still carries a Gaussian-like shape as shown in later section.

The chemical reaction is a result of the collision between a hopping photoacid and the acid-labile functional group in the polymer matrix microscopically. There is a definite relationship between the macroscopic parameter (k_p , D , t) and microscopic parameters such as number of hopping steps (n), average time interval (τ) and step length (L) and the reaction probability (α) for each collision with acid-labile group¹⁸. These relationships are summarized in Table 2. With these formulas, PBF can be dimensionless if the distance r is in the unit of step length L .

$$PBF = 1 - \exp[-(3\alpha / 2\pi) \text{erfc}(r\sqrt{3/2n}) / r] \quad (6)$$

It can be seen that “ Dt ” has been incorporated into one variable, the number of hopping steps “ n ” and only one parameter, the reaction probability per collision “ α ”, is left in this *PBF*. The hopping step length only appears as a scaling factor for distance. The detailed implication of equation (6) will be discussed in later section.

Table 1. Parameter used in the simulation (standard processing conditions)

| | |
|---|---|
| Dill parameter (cm ² /mJ) | C = 0.11 |
| Initial PAG concentration (nm ⁻³) | PAG0 = 0.048 (4% mass fraction) |
| Exposure dose (mJ/cm ²) | E = E ₀ [1-ε cos(2πx/L ₀)] E ₀ = 7.0; ε = 1.0; L ₀ = 280 nm |
| Deprotection reaction constant | k _p = 10 |
| Trapping constant (nm ³ /s) | k _T = 0.2 |
| Diffusion coefficient (nm ² /s) | D = 20 |
| PEB time (s) | t = 90 |

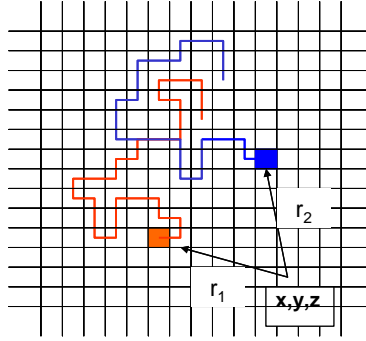


Figure 1. Microscopic picture of reaction-diffusion of photoacid taking random-walk in photoresists polymer matrix.

Table 2. Conversion of microscopic to macroscopic parameters for random-walk type reaction-diffusion.

| Macroscopic parameters | Microscopic parameters | Macro- to micro- parameter conversion |
|------------------------|------------------------|---|
| k_p, D, t | α, n, τ, L | $t = n\tau; D = \frac{L^2}{6\tau}; k_p = \frac{\alpha L^3}{\tau}$ |

When multiple photoacids are present, the concentration shown in equation (4) is addable and the total reaction extent or deprotection level can be calculated as

$$\phi(x, y, z) = 1 - \exp[-k_p / 4\pi D \sum_{PAGi} \text{erfc}(r_i / \sqrt{4Dt_i}) / r_i] \quad (7)$$

Here the r_i and t_i are the distance of a PAG's initial position to a reference point (x,y,z) and the PAG's lifetime, respectively. When there is no PAG loss ($k_T = 0$), t_i is a constant equal to the PEB time and equation (7) is an exact

solution for equation (2) and (3). When there is PAG loss, no analytical solution can be found about equation (2) and (3). However we can treat equation (7) as an approximation solution for them, in which the lifetime of each photoacid is different and is less than or equal to PEB time. The procedure of finding the photoacid lifetime is listed as following: a) Generate a certain number of photoacid with distribution satisfying equation (1) to (3) in a given simulation box. b) Calculate the number of photoacid lost at each time interval for a given moment. This determines the lifetime of a certain group of photoacids; c) Assign positions to these acids randomly according to their initial profile.

Due to the diffusive nature of the photoacid, a proper boundary condition must be applied, otherwise the deprotection level simulated will be much lower than expected by a continuum model. To avoid this problem, we defined two boxes: a PAG box and a sampling box. The sampling box is included in the PAG box which is much larger than the former so that all the PAG outside of the PAG box has ignorable contribution to the deprotection reaction in each block inside sampling box.

If projecting all the deprotection level calculated in each sampling block to lateral direction, a fluffy deprotection profile can be obtained, indicating the existence of chemical composition fluctuation at each slice along x-axis. Figure 2 shows the deprotection profiles calculated from continuum model and discrete model discussed above. The general trends for these two profiles agree very well but deviation exists in some position. This is mainly due to the approximation in determining the PAG lifetime and setting boundary conditions. A more sophisticated algorithm can be developed to further improve the approximation.

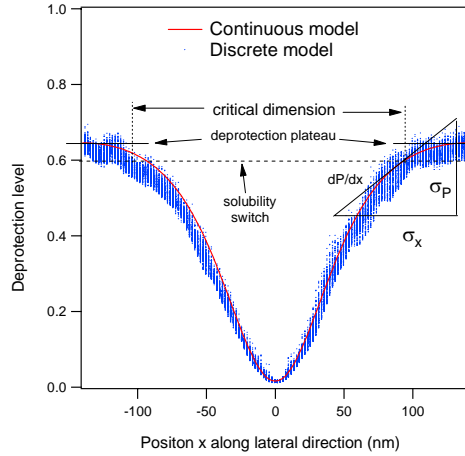


Figure 2. Deprotection profile calculated with continuous model and discrete 3-D model. All conditions are same as listed in table 1 except PEB time = 3 s. The acid loss is about 18 % within this period.

2.2. LER simulation

If we ignore the dissolution kinetics and the swelling/collapse details, LER or spatial fluctuation can be directly attributed to chemical composition fluctuation due to the critical ionization mechanism^{8,9,19}. Using Taylor expansion, the spatial fluctuation is given by

$$\sigma_x = \sigma_p \left(\frac{d\phi}{dx} \right)_{\phi=\phi_0}^{-1} \quad (8)$$

Where the σ_x and the σ_p are the standard deviations of the spatial and the chemical fluctuation respectively. The ϕ_0 is the critical deprotection level that switches the solubility of photoresists. The relationship among them is also shown in Figure 2. Thus the spatial fluctuation or LER is actually the projection of chemical fluctuation on protection gradient direction around solubility switch. Similar ideas were also reported in the literature.^{15,20}

3. Results and discussion

3.1. Point-blur-function.

With equation (5) and (6), we can discuss the spatial distribution of deprotection reaction and how it is affected by various factors. The deprotection region is a sphere in shape but denser in the center in agreement with small angle neutron scattering results²¹. If the deprotection distribution on the plane through the center of the sphere is investigated, a cone shape profile can be shown in Figure 3a, which looks quite similar to the results of Hinsberg and et al.¹¹. Figure 3b and 3c show the deprotection profile for various number of hopping ($n \sim \sqrt{Dt}$) and reaction probability ($\alpha \sim k_p / D$). Increasing either n or α can all spread the deprotection sphere but these two factors behave in different way. The former will form a more fluffy sphere but the later form a more solid sphere. Since photoresist includes more than one PAG, the degree of sphere overlapping determines the overall chemical composition fluctuation or heterogeneity. Increasing n can produce more overlapping, therefore decrease chemical heterogeneity while increasing α will increase heterogeneity.

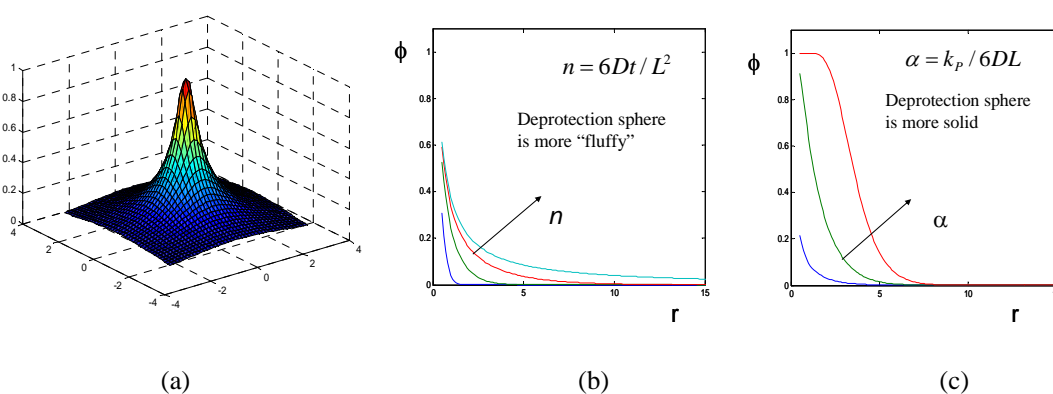


Figure 3. (a)Deprotection profile along the cross-section through the center of deprotection sphere produced by the reaction-diffusion of a single photoacid. (b) Change of deprotection profile by changing number of hopping steps n . (c) Change of deprotection profile by changing reaction probability α .

The same discussion can also be made with macroscopic parameter (k_p , D , t). Increasing k_p is equivalent to increase α , therefore the heterogeneity will increase; increasing D can decrease α and increase n , either way will decrease heterogeneity; increasing t simply increases n , the heterogeneity will decrease.

3.2. Dose and dose contrast

Table 3 shows the simulated chemical composition fluctuation (CCF), deprotection gradient at the solubility switch (DGSS) and LER for various dose and dose contrast while all other conditions are fixed. The aerial image distribution of exposure along wafer plane is shown in Figure 4. Figure 5a and 5b shows the dependence of LER and CCF on DGSS. It can be seen that the LER monotonically increase with dose or dose contrast (Figure 5b) just as expected. However the CCF does not change much when dose or dose contrast is varied. This is rather surprising because higher dose always cause larger overlapping than lower dose. This fact can be understood with the *PBF* discussed in section 3.1 because it only depends on kinetics parameters such as reaction/trapping rate constants, diffusivity and deprotection reaction time. Although the overlapping of deprotection spheres are different for low dose and high dose, the difference of heterogeneity produced by them is only significant at deprotection level around 0.2 to 0.3 just as we have pointed in our recent study.²² When the deprotection level is as high as 0.6 at solubility switch, the difference is ignorable.

Table 3 Calculated deprotection gradient, chemical roughness and LER for standard processing conditions ($E_0 = 7.0$ mJ/cm²; $\varepsilon = 1.0$; $k_p = 10$ nm³/s; $D = 20$ nm²/s; $t = 90$ s; $k_T = 0.2$ nm³/s) and other conditions in which only one or two parameters differ from standard conditions. (Assuming solubility switch = 0.6)

| | | Deprotection Gradient ($\times 10^{-3}/\text{nm}$) | Chemical roughness ($\times 10^{-3}$) | LER(3σ) (nm) |
|--|---------------------|---|--|--------------------------|
| Standard processing Parameters | | $11.3 \pm 1.0^*$ | $10.5 \pm 1.3^*$ | $2.7 \pm 0.5^*$ |
| Changed conditions | | | | |
| Dose (mJ/cm ²) | $E_0 = 2.0$ | 5.9 ± 0.5 | 9.4 ± 1.9 | 4.8 ± 1.0 |
| | $E_0 = 0.7$ | 2.6 ± 0.7 | 9.0 ± 1.8 | 10.5 ± 3.3 |
| Dose contrast at fixed dose $E_0 = 2.0$ mJ/cm ² | $\varepsilon = 0.7$ | 4.7 ± 0.6 | 9.6 ± 1.4 | 6.0 ± 1.2 |
| | $\varepsilon = 0.5$ | 2.9 ± 0.8 | 10.3 ± 2.1 | 10.8 ± 3.6 |
| | $\varepsilon = 0.2$ | 1.3 ± 0.8 | 8.7 ± 2.0 | 19.5 ± 12.9 |
| Reaction constant (nm ³ /s) | $k_p = 20$ | 17.6 ± 0.5 | 23.5 ± 1.6 | 4.0 ± 0.3 |
| Diffusion coefficient (nm ² /s) | $D = 10$ | 12.9 ± 0.8 | 19.9 ± 2.1 | 4.6 ± 0.6 |
| PEB time (s) | $t = 6$ | 7.3 ± 1.3 | 14.3 ± 2.4 | 6.0 ± 1.5 |
| Trapping constant (nm ³ /s) | $k_T = 0.5$ | 3.4 ± 1.5 | 13.7 ± 2.9 | 12.0 ± 6.0 |

* The error which is produced by sampling fluctuation is corresponding to one standard deviation from fitting linear regression model.

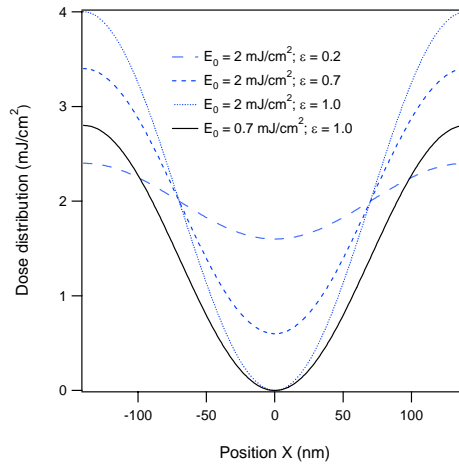


Figure 4. Exposure energy distribution along wafer plane

Since the CCF (σ_p) is relatively constant for various dose and dose contrast, the LER will be inversely proportional to DGSS according to equation (8). Therefore, the LER is only a function of DGSS independent of the dose and dose contrast. This conclusion agrees with that reported in literature³.

Increasing dose or dose contrast to reduce LER is a well known fact. However, this is mainly due to the increase of the DGSS instead of the decrease of shot-noise or statistical fluctuation as expected. A detailed investigation on deprotection profile further shows that large LER or small DGSS mostly occur when the deprotection level at a plateau region of the profile is close to the solubility switch. Smaller LER always appear when deprotection level at plateau region is far above solubility switch. Figure 6 shows that a roughly monotonic relationship exists between the DGSS and the difference between the deprotection level at a plateau region and the solubility switch. Figure 6 also suggests that either increasing the plateau deprotection level (by increasing dose) or decreasing solubility switch (by changing developer) all help decrease LER.

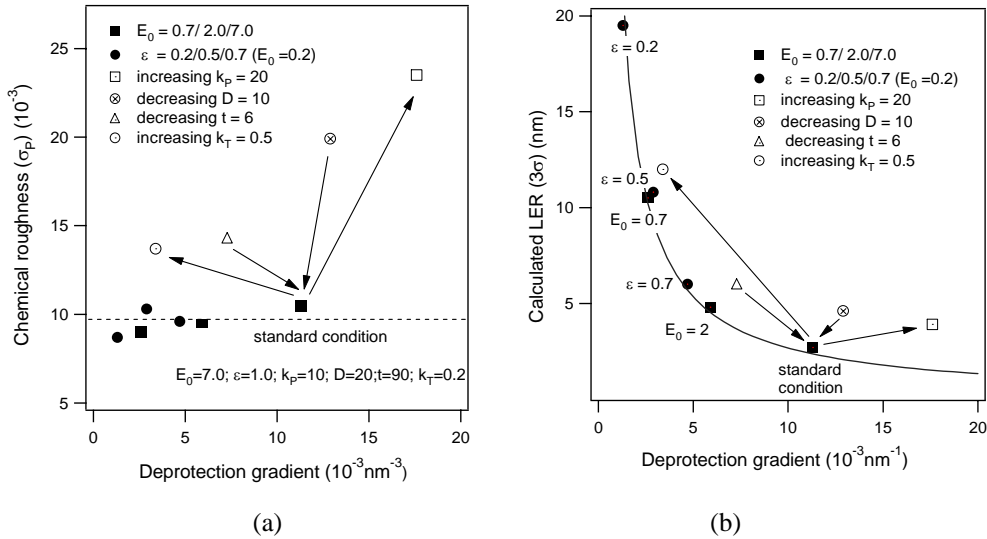


Figure 5. Simulated chemical composition fluctuation (chemical roughness) (a) and LER (b) vs. deprotection gradient for standard processing conditions and other conditions in which one parameter differs from the standard conditions. The line is drawn to guide the reader's eyes. The data are also shown in Table 3.

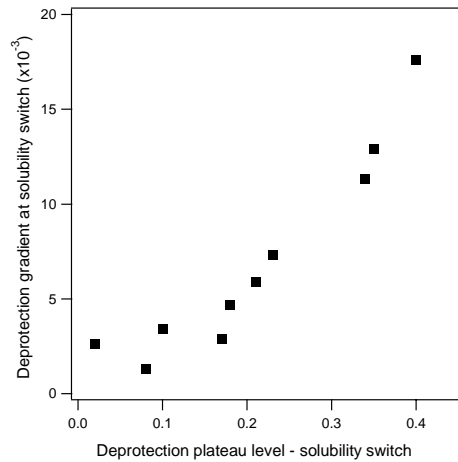


Figure 6. Deprotection gradient at solubility switch vs. the difference between deprotection plateau and solubility switch.

3.3. Reaction constant, trapping constant, PEB time and diffusion coefficient on LER

Table 3 also shows the CCF, DGSS and LER by changing the reaction constant, diffusion coefficient, PEB time and trapping constant. The relationship between CCF vs. DGSS and LER vs. DGSS is shown in Figures 5a and 5b.

When compared to the standard processing condition, increasing the reaction constant or trapping constant and decreasing PEB time or diffusion coefficient all induce a larger chemical roughness and LER. The trend is shown by the arrows to and from the standard condition in Fig. 5. The effect on chemical roughness from these factors can be understood based on the knowledge of *PBF* because they can cause either a decrease of hopping number ($n \sim \sqrt{Dt}$) or an increase of the reaction probability ($\alpha \sim k_p / D$). The effects of the above parameters on DGSS are more complicated and subtle; DGSS is mainly affected by the relative distance between the deprotection plateau level (DPL) and the solubility switch according to Figure 6. When solubility switch is fixed, the DGSS is mostly determined by DPL. Figure 3b and 3c show that the deprotection level produced by each photoacid monotonically increase with n and α . Therefore the DPL and the DGSS are also dictated by n and α in addition to dose and dose contrast. With this knowledge we can further discuss the effects on LER from above parameters.

The summary of the relationship between these parameters with CCF and DGSS are shown in Table 4. For example, by increasing k_p both CCF and DGSS increase because α increases. However the effect on CCF is stronger, the net result is that the LER increases. Increasing k_T or decreasing the PEB time (more accurately the deprotection reaction time because most of acid have become inactive before the PEB time) leads to a decreased DGSS and CCF because of their effect on n . Decreasing the diffusion coefficient usually makes the DGSS larger, which seems to imply the LER becomes smaller. However, decreasing diffusion coefficient causes a more significant effect on CCF, therefore the overall LER still increases. This relationship regarding the PAG diffusivity and the LER has been experimentally observed according to published literature.^{20,23}

Table 4. Relationship about processing parameters and LER. $\alpha \sim k_p / D$ and $n \sim \sqrt{Dt}$ where the t is the deprotection reaction time instead of actual PEB time. Increasing k_T can effectively shorten the average reaction time.

| | | | | |
|--|-----------------|------------------|---------------|------------------------------------|
| $LER = \frac{CCF(\alpha, n)}{DGSS(\alpha, n, E_0, \varepsilon)}$ | CCF \uparrow | $\alpha\uparrow$ | $n\downarrow$ | |
| | DGSS \uparrow | $\alpha\uparrow$ | $n\uparrow$ | $E_0\uparrow, \varepsilon\uparrow$ |

Although changing some factors is favorable to minimize LER, there is usually a limitation imposed by the photoresist polymer or PAG material on the pattern such as resolution or critical dimension. Theoretically, increasing diffusion coefficient or PEB time can all decrease LER, but this will also decrease the pitch size or critical dimension which is unwanted in photoresist design. To overcome this problem, base quencher has to be added to counteract the diffusion effect. Adding base quencher can increase the DGSS if the deprotection plateau is not significantly decreased (this case happens when dose is high enough), but the CCF is also increased due to the reduced lifetime or deprotection reaction time of photoacids. Thus the overall gain to LER minimization is still limited.

4. Conclusion

A 3-D latent image is calculated by combining the continuum diffusion-reaction equation with the random-walk mechanism of individual PAG in photoresist matrix and the resulting LER has been estimated for various processing factors. It has been shown that the LER depends on both deprotection gradient and chemical composition fluctuation. When the dose or dose contrast is varied, the chemical composition fluctuation is relatively constant so that the LER is mainly dictated by deprotection gradient and approximately inversely proportional to it. When other factors such as the reaction rate constant, PEB time, trapping constant, and diffusivity are varied, the chemical composition roughness is also changed, which makes the LER deviate from the inverse relationship to deprotection gradient. The chemical composition fluctuation can be illustrated with point blur function which is dictated by the number of hopping (n) and the reaction probability (α) of photoacid. The deprotection gradient is mainly determined by the difference between solubility switch and deprotection plateau level which is also dependent on the n and the α .

5. Acknowledgements

This work was supported by SEMATECH under Agreement #309841 OF.

References

1. He, D.; Cerrina, F. Process dependence of roughness in a positive-tone chemically amplified resist. *J Vac Sci Techn B* **1998**, *16* (6), 3748-3751.
2. Hinsberg, W.; Houle, F. A.; Hoffnagle, J.; Sanchez, M.; Wallraff, G.; Morrison, M.; Frank, S. Deep-ultraviolet interferometric lithography as a tool for assessment of chemically amplified photoresist performance. *J Vac Sci Techn B* **1998**, *16*, 3689-3694.
3. Pawloski, A.; Acheta, A.; Levinson, H.; Michaelson, T. B.; Jamieson, A.; Nishimura, Y.; Willson, C. G. Line edge roughness and intrinsic bias for methacrylic polymer resist systems. *J. Microlith. , Microfab. , Microsyst.* **2006**, *5* (2), 023001-1-023001-16.
4. Shin, J.; Han, G.; Ma, Y.; Moloni, K.; Cerrina, F. Resist line edge roughness and aerial image contrast. *J Vac Sci Techn B* **2001**, *19* (6), 2890-2895.
5. Reynolds, G. W.; Taylor, J. W. Factors contributing to sidewall roughness in a positive-tone, chemically amplified resist exposed by x-ray lithography. *J Vac Sci Techn B* **1999**, *17* (2), 334-344.
6. Shin, J.; Ma, Y.; Cerrina, F. Depth dependence of resist line-edge-roughness:relation to photoacid diffusion length. *J Vac Sci Techn B* **2002**, *20* (6), 2927-2931.
7. Houle, F. A.; Hinsberg, W. D.; Sanchez, M. I. Kinetics model for positive tone resist dissolution and roughening. *Macromolecules* **2002**, *35*, 8591-8600.
8. Houle, F. A.; Hinsberg, W. D.; Sanchez, M. I. Acid-base reactions in a positive tone chemically amplified photoresist and their effect on imaging. *Journal of Vacuum Science & Technology B* **2004**, *22* (2), 747-757.
9. Tsiartas, P. C.; Flanagan, L. W.; Henderson, C. L.; Hinsberg, W. D.; Sanchez, I. C.; Bonnacaze, R. T.; Willson, C. G. The mechanism of phenolic polymer dissolution: A new perspective. *Macromolecules* **1997**, *30* (16), 4656-4664.
10. Gallatin, G. M. Resist blur and line-edge-roughness. *Proceedings of the SPIE - The International Society for Optical Engineering* **2005**, *5754*, 38-52.
11. Hinsberg, W. D.; Houle, F. A.; Sanchez, M.; Hoffnagle, J.; Wallraff, G.; Medeiros, D.; Gallatin, G. M.; Cobb, J. Extendibility of chemically amplified resists: another brick wall? *Proceedings of the SPIE - The International Society for Optical Engineering* **2003**, *5039*, 1-14.
12. Meiring, J. E.; Michaelson, T. B.; Jamieson, A.; Schmid, G.; Willson, C. Using Mesoscale simulation to explore photoresist line edge roughness. *Proceedings of the SPIE - The International Society for Optical Engineering* **2005**, *5753*, 350-360.
13. Schmid, G. M.; Stewart, M. D.; Singh, V. K.; Willson, C. G. Spatial distribution of reaction products in positive tone chemically amplified resists. *Journal of Vacuum Science & Technology B* **2002**, *20* (1), 185-190.
14. Schmid, G. M.; Stewart, M. D.; Burns, S. D.; Willson, C. G. Mesoscale Monte Carlo simulation of photoresist processing. *Journal of the Electrochemical Society* **2004**, *151* (2), G155-G161.
15. Smith, M. D. Mechanistic model of line edge roughness. *Proceedings of the SPIE - The International Society for Optical Engineering* **2006**, *6153*, 61530X-1-61530X-9.

16. Pawloski, A.; Acheta, A.; Lalovic, I.; LaFontaine, B.; Levinson, H. Characterization of line edge roughness in photoresist using an image fading technique. *Proceedings of the SPIE, Advances in Resist Technology and Processing XXI* **2004**, 5376, 414.
17. Kang, S.; Prabhu, V. M.; Vogt, B. D.; Lin, E. K.; Wu, W. L.; Turnquest, K. Effect of copolymer composition on acid-catalyzed deprotection reaction kinetics in model photoresists. *Polymer* **2006**, 47, 6293-6302.
18. Nakamura, J.; Ban, H.; Tanaka, A. influence of acid diffusion on the lithographic performance of chemically amplified resists. *Jpn. J. Appl. Phys.* **1992**, 31, 4294-4300.
19. Burns, S. D.; Schmid, G. M.; Tsiartas, P. C.; Willson, C. G. Advancements to critical ionization dissolution model. *J Vac Sci Techn B* **2002**, 20 (2), 537-543.
20. Yoshizawa, M.; Moriya, S. Study of the acid-diffusion effect on line edge roughness using the edge roughness evaluation method. *J Vac Sci Techn B* **2002**, 20 (4), 1342-1347.
21. Jones, R. L.; Hu, T. J.; Lin, E. K.; Wu, W. L.; Goldfarb, D. L.; Angelopoulos, M.; Trinque, B. C.; Schmid, G. M.; Stewart, M. D.; Willson, C. G. Formation of deprotected fuzzy blobs in chemically amplified resists. *Journal of Polymer Science Part B-Polymer Physics* **2004**, 42 (17), 3063-3069.
22. Kang, S.; Vogt, B. D.; Wu, W. L.; Prabhu, V. M.; Vanderhart, D.; Rao, A.; Lin, E. K. Characterization of compositional heterogeneities in chemically amplified photoresists thin films with infrared spectroscopy. *Macromolecules* **2007**, 40, 1497-1503.
23. Steenwinckel, D. V.; Lammers, J. H.; Leunissen, L. H.; Kwinten, J. A. Lithographic importance of acid diffusion in chemically amplified resists. *Proceedings of the SPIE - The International Society for Optical Engineering* **2005**, 5753, 269-280.